# Experimental Hypersonic Aerodynamic Characteristics of the Space Shuttle Orbiter for a Range of Damage Scenarios

Gregory J. Brauckmann[*] and William I. Scallion[†]
*NASA Langley Research Center, Hampton, VA 23681*

Aerodynamic tests in support of the Columbia accident investigation were conducted in two hypersonic wind tunnels at the NASA Langley Research Center, the 20-Inch Mach 6 Air Tunnel and the 20-Inch $CF_4$ Tunnel. The primary purpose of these tests was to measure the forces and moments generated by a variety of outer mold line alterations (damage scenarios) using 0.0075-scale models of the Space Shuttle Orbiter. Simultaneously acquired global heat transfer mappings were obtained for a majority of the configurations tested. Test parametrics included angles of attack from 38 to 42 deg, unit Reynolds numbers from 0.3 $x10^6$ to 3.0 $x10^6$ per foot, and normal shock density ratios of 5 (Mach 6 air) and 12 ($CF_4$). The damage scenarios evaluated included asymmetric boundary layer transition, gouges in the windward surface thermal protection system tiles, wing leading edge damage (partially and fully missing reinforced carbon-carbon (RCC) panels), deformation of the wing windward surface, and main landing gear and/or door deployment. The measured aerodynamic increments for the damage scenarios examined were generally small in magnitude, as were the flight-derived values during most of the entry prior to loss of communication. A progressive damage scenario is presented that qualitatively matches the flight observations for the STS-107 entry.

## I.    Nomenclature

| | | |
|---|---|---|
| H | = | depth of main landing gear wheel well |
| L | = | length of main landing gear wheel well |
| LB | = | Orbiter reference body length |
| $\Delta CA$ | = | delta axial-force coefficient |
| $\Delta Cl$ | = | delta rolling-moment coefficient |
| $\Delta Cm$ | = | delta pitching-moment coefficient |
| $\Delta CN$ | = | delta normal-force coefficient |
| $\Delta Cn$ | = | delta yawing-moment coefficient |
| $\Delta CY$ | = | delta side-force coefficient |
| $M_\infty$ | = | freestream Mach number |
| $q_\infty$ | = | freestream dynamic pressure, psi |
| $P_{t,1}$ | = | reservoir pressure, psi |
| $Re_\infty$ | = | freestream unit Reynolds number, $ft^{-1}$ $10^{-6}$ |
| $Re_{\infty,LB}$ | = | freestream length Reynolds number (based on Orbiter reference length), $10^{-6}$ |
| $T_{t,1}$ | = | reservoir temperature, °R |
| $X_{bar}$ | = | longitudinal moment arm |
| $X_{mrc}$ | = | longitudinal moment reference center |
| $Y_{bar}$ | = | lateral moment arm |
| $Z_{bar}$ | = | vertical moment arm |
| $\alpha$ | = | angle of attack, degrees |
| $\beta$ | = | angle of sideslip, degrees |
| $\gamma_\infty$ | = | freestream ratio of specific heats |

[*] Senior Researcher, Aerothermodynamics Branch, MS 408A, Associate Fellow AIAA.
[†] Senior Researcher, Aerothermodynamics Branch, MS 408A, Senior Member AIAA.

$\rho_\infty$       = freestream density, sl/ft$^3$
$\rho_2$        = post-normal shock density, sl/ft$^3$

## II.  Introduction

THE Space Shuttle Columbia suffered catastrophic failure during entry on February 1, 2003. The Orbiter was traveling at a speed corresponding to approximately Mach 18 at an altitude of 201,000 feet when loss of signal occurred. An investigation into the cause of the accident was immediately initiated, culminating in the Columbia Accident Investigation Board's (CAIB) finding that the physical cause was a debris strike during ascent (foam insulation from the bipod ramp of the external tank) damaging the left wing leading edge which caused a breach allowing hot gas into the wing interior during entry. This hot gas progressively weakened the internal structure of the wing, leading to loss of aerodynamic control and eventual breakup of the orbiter[1]. The final CAIB report incorporated the results of analyses by many teams and individuals, representing work in the various disciplines of aerodynamics, aerothermodynamics, structures, and others. This paper presents a portion of the aerodynamic results, from wind tunnel tests conducted in two hypersonic wind tunnels at the NASA Langley Research Center. The primary purpose of the tests was to measure the aerodynamic forces and moments generated by a variety of outer mold line alterations (damage scenarios) and compare the results to the observed aerodynamic behavior of Columbia during its final flight. Complementary global heat transfer mappings were simultaneously acquired to aid the aerodynamic study via determination of boundary layer transition, and to qualitatively assess the aerodynamic heating effects of the various damage scenarios.

The order in which the results are presented in this paper loosely correspond to the course of the investigation, from an aerodynamic and external aerothermodynamic standpoint, as the focus changed over time as new information became available. The initial information available to investigators after the loss of STS-107 came from two sources, video footage of the foam strike on ascent, and telemetry data from the Orbiter Instrumentation (OI) system, which provided temperature and pressure measurements at various times and locations on the vehicle as well as accelerations with which to reconstruct the vehicle aerodynamic characteristics. These data were later augmented by analyses of the recovered debris, and by more extensive (in terms of locations, data acquisition rate, type of measurements) measurements from the Modular Auxiliary Data System (MADS) when its' recorder was recovered approximately seven weeks after the accident.

The un-enhanced ascent video indicated a debris strike on the left wing of Columbia somewhere between the wing leading edge and the main landing gear (MLG) door. The OI data indicated off-nominal temperature and pressure measurements in the left main landing gear wheel well beginning 490 seconds after entry interface (EI), off-nominal aerodynamic moments beginning about 515 seconds after EI (primarily a left-wing down rolling moment and a nose-left yawing moment), and off-nominal measurements of side fuselage bond-line (i.e. region of TPS attachment to the underlying structure) temperatures (resistance temperature devices (RTDs) V34T1106A and V09T1724A) at fuselage stations 1215 and 1410 beginning 613 seconds after EI. The timing of the off-nominal side fuselage heating at 613 seconds corresponds to a change in the rolling moment trend from left-wing down to right-wing down. These initial observations led to tests in the 20-Inch Mach 6 Air Tunnel to examine the aerodynamic and aerothermodynamic effects of damage to the thermal protection system (TPS) tiles on the windward surface of the left wing, asymmetric boundary layer transition effects, and possible main landing gear and door deployment. Just prior to the start of these tests, results from both an inviscid Euler code and an initial series of experimental aeroheating tests showed that damage to the wing leading edge in the form of a missing reinforced carbon-carbon (RCC) panel would result in an increase in pressure and heating to the side of the fuselage similar to that observed for the side fuselage RTD's. Subsequent testing in the 20-Inch CF$_4$ Tunnel (which simulated Mach 18 to 24 flight conditions via use of a heavier-than-air test gas providing a lower ratio of specific heats) focused on damage to the wing leading edge consisting of missing RCC panels, singly and in combinations. As the recovered debris indicated that a completely missing RCC panel was unlikely, at least early in flight, partially missing RCC panels were investigated by removing the lower section of the panel. Additional tests investigated alternate paths for flow to reach the leeside such as holes and slots through the carrier panel behind RCC panel 8. As the flight aerodynamic moments were refined it became apparent, that due to uncertainties in both the flight aerodynamic and wind tunnel measurements, aerodynamics would not be a major discriminator of possible damage scenarios for earlier times in the flight. Attention then shifted to possible causes of the reversal in the rolling moment trend which occurred at 615 seconds after EI and the large moments late in flight just prior to the time of loss of signal (LOS). The effect of flow impinging on the vertical tail was isolated, and a windward deformation of the left wing in the form of a series of grooves, representing a depressed lower surface, was tested. To tie all the results together into a viable scenario, a progressive series of damages beginning with a lower missing RCC panel 8 and ending with a deformed lower wing

surface was assembled from the experimental results which qualitatively matched the flight aerodynamic moments and thermal events.

## III.   FACILITIES, MODELS, AND TEST TECHNIQUES

### A. Facilities

The two facilities used in this investigation were the Langley 20-Inch Mach 6 Air Tunnel and the Langley 20-Inch $CF_4$ Tunnel[2]. These facilities are conventional (as compared to impulse), low-enthalpy, blow-down type hypersonic tunnels. The Mach 6 air tunnel uses heated, dried, and filtered air as the test gas. Typical operating conditions for the tunnel are: stagnation pressures from 30 to 500 psia; stagnation temperatures from 760 to 1000°R, free stream Mach number from 5.8 to 6.1; free stream unit Reynolds numbers from 0.5 to 8 million per foot; a free stream and post-normal shock ratio of specific heats (gamma, $\gamma$) of 1.4; and a normal shock density ratio of 5.3. The facility has a two-dimensional contoured nozzle leading to a closed, solid-wall test section with dimensions of 20.5 by 20 inches. The test core varies from 12 to 14 inches depending on the operating condition. Nominal run time is approximately 60 to 120 seconds, although longer runs times are possible.

The $CF_4$ Tunnel uses heated, dried, and filtered carbon tetraflouride (Freon 14; molecular weight of 88 which is three times heavier than air) as the test gas. Typical operating conditions for the tunnel are: stagnation pressures from 85 to 2000 psia; stagnation temperatures up to 1300°R, free stream Mach number from 5.9 to 6.0; free stream unit Reynolds numbers from 0.02 to 0.55 million per foot; a free stream gamma of 1.21 and a post-normal shock gamma of 1.10; and a normal shock density ratio of 11.7. The facility has a contoured axi-symmetric nozzle with a nozzle exit diameter of 20 inches, leading to an open-jet test section. The test core varies from 12 to 14 inches depending on the operating condition. Nominal run time is approximately 20 seconds.

The loss of STS-107 occurred during entry at high Mach number and enthalpy levels, and relatively low Reynolds numbers. At these flight conditions high-temperature effects (i.e. flow chemistry) are significant due to the dissociation-recombination and ionization of the gas as it passes through the vehicle bow and wing shocks. These high-temperature effects increase the shock density ratio and lower the specific heat ratio (gamma) of the gas within the shock layer, causing shocks to lie closer to the vehicle surface thereby altering their interaction locations; these high-temperature effects cause the gas to expand to lower pressures than would occur for a non-reacting gas. The $CF_4$ tunnel provides a simulation of these high-temperature effects via its low value of gamma, which is near the value within the Orbiter windward flow field at hypervelocity flight conditions. For example, lower pressure levels than expected on the aft windward portion of the Orbiter were identified as the root cause of the Orbiter "pitch-up anomaly" that occurred during the first flight of Columbia, STS-1, wherein the Orbiter experienced a nose-up pitch increment relative to pre-flight predictions. The $CF_4$ tunnel has been used to successfully demonstrate the magnitude and direction of this pitch-up increment[3]. While the ability of the $CF_4$ tunnel to accurately simulate the leeside flow of the Orbiter at hypervelocity conditions has not been validated to the extent of the windward flow, the damage scenarios investigated have their initiation on the wing leading edge and the windward surface, and thus the $CF_4$ tunnel is expected to provide credible simulation of their effects. The Mach 6 air tunnel uses a perfect gas, but all the flow physics phenomena such as flow separation-reattachment, boundary layer transition, and shock-shock interactions, will be present. The high-temperature effects may alter the level and location of these phenomena, but should not add or delete from them. The Mach 6 air tunnel, which is highly productive, was thus used in a preliminary or screening role with the $CF_4$ tunnel used to refine the results. In addition, the Mach 6 air tunnel was used for the boundary layer transition studies since it had been used extensively in the past for such studies on the Shuttle Orbiter[4,5]. A more detailed discussion of the use of these facilities and their relation to the flight environment can be found in Ref. 6.
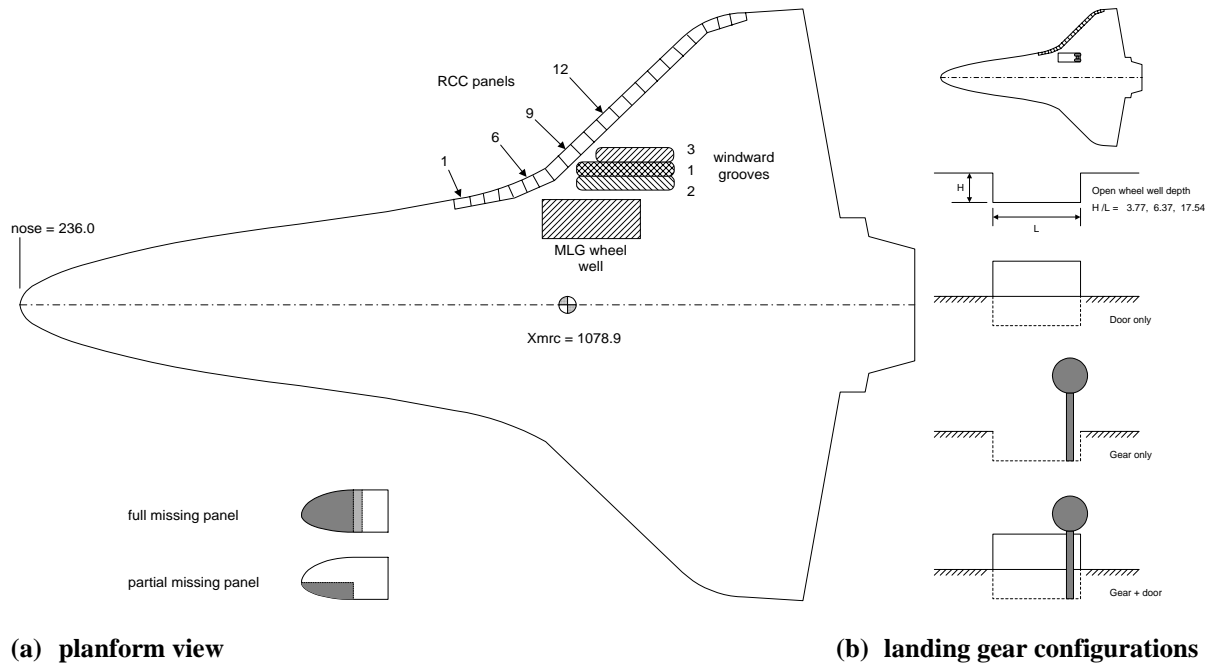
The flow conditions in the two facilities for the tests performed for this investigation are summarized in Table 1 below. The majority of the runs in the Mach 6 air tunnel were made at a length Reynolds number ($Re_{\infty, LB}$) of 2.4 million, which matched the flight value at Mach 19 and 207,00 feet, near loss of signal. The majority of the runs in the $CF_4$ tunnel were made at a length Reynolds number of 0.4 million, which matched the flight value at Mach 25 and 256,000 feet.

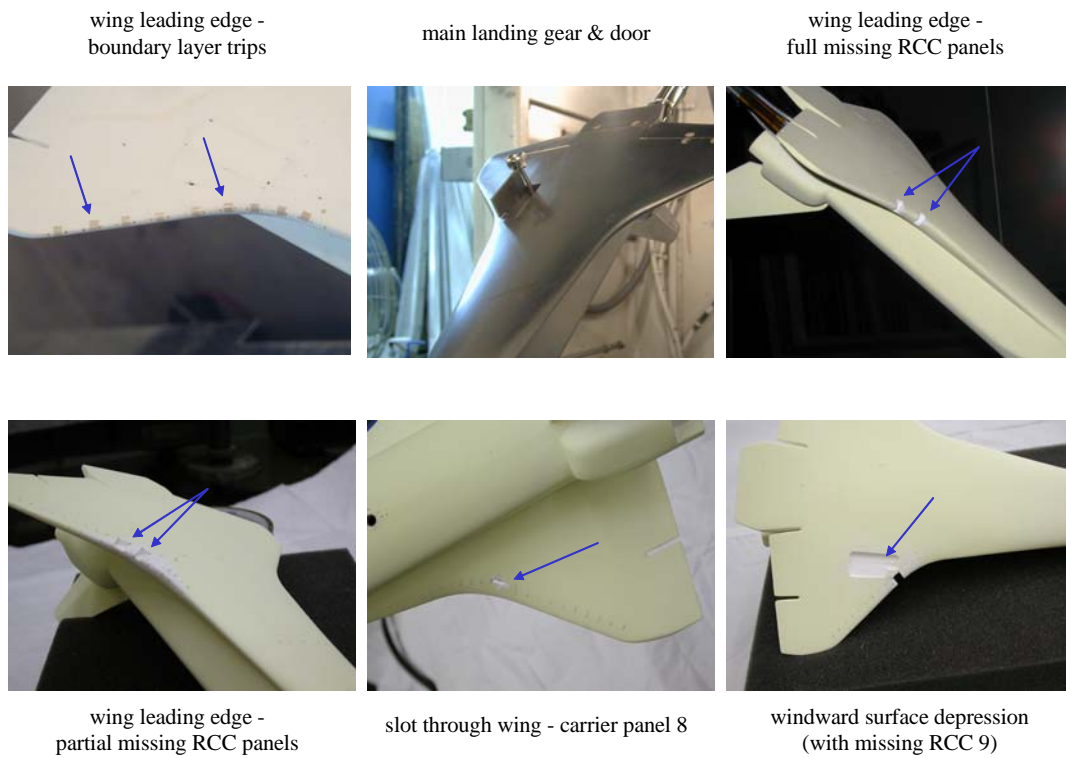Table 1. Nominal Flow Conditions in NASA LaRC Aerothermodynamics Laboratory

| Facility | $P_{t,1}$ (psi) | $T_{t,1}$ (°R) | $M_\infty$ | $q_\infty$ (psi) | $Re_\infty$ (ft$^{-1}$) | $\rho_2/\rho_\infty$ | $\gamma_\infty$ |
|---|---|---|---|---|---|---|---|
| 20-Inch Mach 6 Air | 60 | 890 | 5.90 | 1.04 | 1.0 | 5.2 | 1.40 |
| | 125 | 910 | 5.94 | 2.10 | 2.1 | 5.3 | 1.40 |
| | 180 | 910 | 5.96 | 3.05 | 3.0 | 5.3 | 1.40 |
| 20-Inch CF$_4$ | 750 | 1180 | 5.94 | 0.65 | 0.27 | 11.7 | 1.22 |
| | 1330 | 1210 | 5.94 | 1.27 | 0.45 | 11.7 | 1.21 |

## B. Wind Tunnel Models

The force-and-moment models used in this investigation were made from either stainless steel or cast silica ceramic. The steel model was an existing 0.0075-scale model that was modified to allow testing of gear and door deployment. A wheel well with a maximum depth of 0.35 inches was machined into the wing, a door was fabricated with a tab to allow installation on the model, and a simplified gear was constructed consisting of a single rod ending in a wheel assembly. The ceramic models were built from a mold using the steel model as a pattern. Individual models were slip cast[7,8], and then a steel sleeve was bonded to the inside to accept the strain-gage force balance. The locations of the RCC and carrier panels were marked on the ceramic models using a coordinate measurement system. Individual missing panels were removed using the location marks as a guide. Fully missing panels, as well as partial panels, where the lower surface from the wing apex to the carrier panel, were removed. Removal of the RCC panel(s) resulted in a "notch" with solid walls, allowing no flow into the interior of the wing leading edge, unlike the actual Orbiter which has a hollow leading edge (open space between the RCC panels and the front wing spar). Other alterations included grooves milled into the windward surface outboard of the wheel well. These grooves were tested sequentially by first lengthening the initial groove, then widening the groove inboard to the wheel well, then outboard. A sketch of the Orbiter windward surface with the various alterations is shown in Fig. 1a, and the gear configurations in Fig. 1b. The longitudinal moment reference center for the aerodynamic data is also shown. Photographs of some of the models are shown in Fig. 2. All models had zero degree control surface deflections of the elevons, body flap, and rudder. Although the control surfaces were deflected in flight, non-deflected control surfaces were used for simplicity, and the data is presented in terms of changes, or deltas, from a nominal configuration. In addition, the gap between the inboard and outboard elevons was not present on the steel model, but was included for the ceramic models.

RCC panels
12
9
6
1
3
1
2
windward grooves
MLG wheel well
nose = 236.0
Xmrc = 1078.9
full missing panel
partial missing panel

H
L
Open wheel well depth
H/L = 3.77, 6.37, 17.54
Door only
Gear only
Gear + door

**(a) planform view**

**(b) landing gear configurations**

**Figure 1.    Sketch of Orbiter with various OML alterations**



wing leading edge -
boundary layer trips

main landing gear & door

wing leading edge -
full missing RCC panels

wing leading edge -
partial missing RCC panels

slot through wing - carrier panel 8

windward surface depression
(with missing RCC 9)

**Figure 2.    Wind tunnel model configurations**

## C.  Test Techniques

Force and moment measurements were obtained using a six-component water-cooled balance. The balance was selected to maximize accuracy of the lateral-directional data. One balance was used for the steel model and another for the lighter-weight ceramic models. Usual corrections for balance interactions, weight tares, and sting bending were made. A baseline (no damage, zero degree control surface deflections) set of aerodynamic coefficients was established for each model over an angle-of-attack range from 38° to 42°. The model was then removed from the balance, modified to provide a damage scenario, re-installed on the balance, and the tests repeated. The baseline data were then subtracted from the subsequent data with the different damage scenarios to provide the incremental aerodynamic forces and moments.

The global heat-transfer mappings were obtained in the Mach 6 air tunnel using an infrared (IR) imaging system[9], while the global mappings obtained in the $CF_4$ tunnel were generated with the two-color relative-intensity phosphor thermography technique[10, 11], as IR techniques are not applicable in the $CF_4$ tunnel because the Freon gas absorbs infrared radiation. In both situations the model surface temperature is the measured quantity and the global heat-transfer images are computed assuming one-dimensional semi-infinite heat conduction. The advantage of these techniques is their non-intrusive and global resolution of the quantitative heat-transfer data. These thermography techniques were used to identify the heating footprints associated with complex, three-dimensional flow phenomena such as boundary layer transition locations, flow separation and reattachment locations, etc. that would be extremely difficult to resolve using discrete measurement techniques. Figure 3 shows a ceramic model installed in the two facilities. The IR camera can be seen above the Mach 6 air tunnel (photograph on left). A similar camera placement was used in the $CF_4$ tunnel, as well as a side-mounted camera for many of the runs.
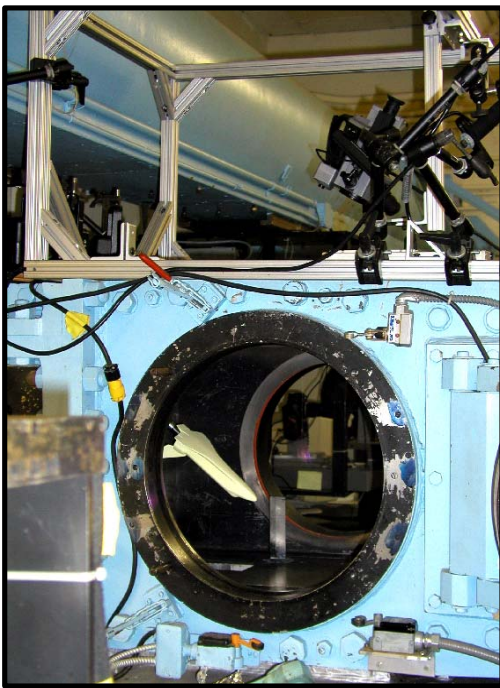


(a)  20-Inch Mach 6 Air Tunnel

(b)  20-Inch $CF_4$ Tunnel

Figure 3.    Photographs of models installed in the 20-Inch Mach 6 Air and 20-Inch $CF_4$ Tunnels

**D. Data Uncertainty**

The uncertainty of the wind tunnel data was estimated in three ways; as an average of the repeatability of the baseline runs for each model, as an average of the repeatability for 8 configurations with leading edge alterations, and as the uncertainty using the balance calibration (laboratory setting). The results are given in Table 2 and are expressed in terms of 2-sigma values of the aerodynamic moment coefficients. The steel model was tested using the same balance in both facilities. This same balance was used for the ceramic models in the 20-Inch Mach 6 Air Tunnel, while the ceramic models tested in the 20-Inch $CF_4$ Tunnel used a smaller-load balance.

Table 2: Uncertainty estimates for the wind tunnel aerodynamic coefficients

| Facility | Configuration | Model | $Re_\infty$ $f^{t-1}$ | $\Delta Cl$ | $\Delta Cn$ | $\Delta Cm$ | $\Delta CN$ | $\Delta CA$ | $\Delta CY$ |
|---|---|---|---|---|---|---|---|---|---|
| Mach 6 Air | baseline | steel | 3.0 | 0.00003 | 0.00006 | 0.00072 | 0.0016 | 0.0003 | 0.0001 |
| Mach 6 Air | baseline | ceramic | 3.0 | 0.00007 | 0.00008 | 0.00044 | 0.0027 | 0.0001 | 0.0001 |
| Mach 6 Air | calibration | balance | 3.0 | 0.00006 | 0.00003 | 0.00048 | 0.0006 | 0.0003 | 0.0003 |
| $CF_4$ | baseline | steel | 0.46 | 0.00010 | 0.00007 | 0.00035 | 0.0077 | 0.0005 | 0.0017 |
| $CF_4$ | baseline | ceramic | 0.46 | 0.00009 | 0.00012 | 0.00042 | 0.0027 | 0.0004 | 0.0005 |
| $CF_4$ | altered | ceramic | 0.46 | 0.00023 | 0.00023 | 0.00024 | 0.0039 | 0.0005 | 0.0010 |
| $CF_4$ | calibration | balance | 0.46 | 0.00009 | 0.00007 | 0.00015 | 0.0001 | 0.0001 | 0.0002 |

## IV.    RESULTS AND DISCUSSIONS

**A. Flight residual aerodynamics**

All comparisons between flight and wind tunnel results presented in this paper are in terms of deltas or increments from a nominal state. In regards to the wind tunnel data the nominal state is a baseline (no damage) run as discussed in the previous section. The incremental flight aerodynamic forces and moments were defined using an iterative approach[12]. The known state of the Orbiter (vehicle attitude, trajectory parameters, vehicle mass properties, control surface position, and on-board measured angular rates) was used as input to a look-up routine in the Orbiter data book to define the nominal aerodynamic coefficients. Next, on-board measured accelerations and angular rates were used with the equations of motion to define the flight aerodynamic coefficients. The differences between these two sets of data (flight, nominal) were the delta aerodynamic coefficients attributed to whatever damage was sustained by the Orbiter. These results were then used as input in a trajectory simulation that included other sources of aerodynamic moments such as winds and atmospheric uncertainties. When a good match was obtained between the trajectory simulation and the known flight trajectory, the delta aerodynamic moments were considered "final".

The final incremental flight moments used for comparison to the wind tunnel data (labeled "simulation") are shown in Fig. 4a-b, along with the extracted flight increments. Prior to 500 seconds after entry interface (EI) there were negligible effects on the Orbiter aerodynamics. The non-zero biases seen in the figures for this time period are considered within the uncertainty of the extracted data or were observed in other flights. After 500 seconds there is an increasing nose-left yawing moment, an increasing left-wing-down rolling moment, and an increasing nose-down pitching moment. These gradual trends continue for yawing and pitching moments until about 840 seconds after entry, then increase sharply until loss of signal. The rolling moment trend reverses at about 615 seconds, becoming positive (left-wing-up) at approximately 700 seconds, and increasing sharply near LOS. Forces (normal, axial, and side) were not used as discriminators due to low resolution and other factors. The flight angles of attack, sideslip and bank are shown in Fig. 5. Angle of attack of the Orbiter was near 40° and sideslip angle was less than 1° for most of the flight, except during planned roll reversal maneuvers.

(a) rolling moment

(b) pitching moment
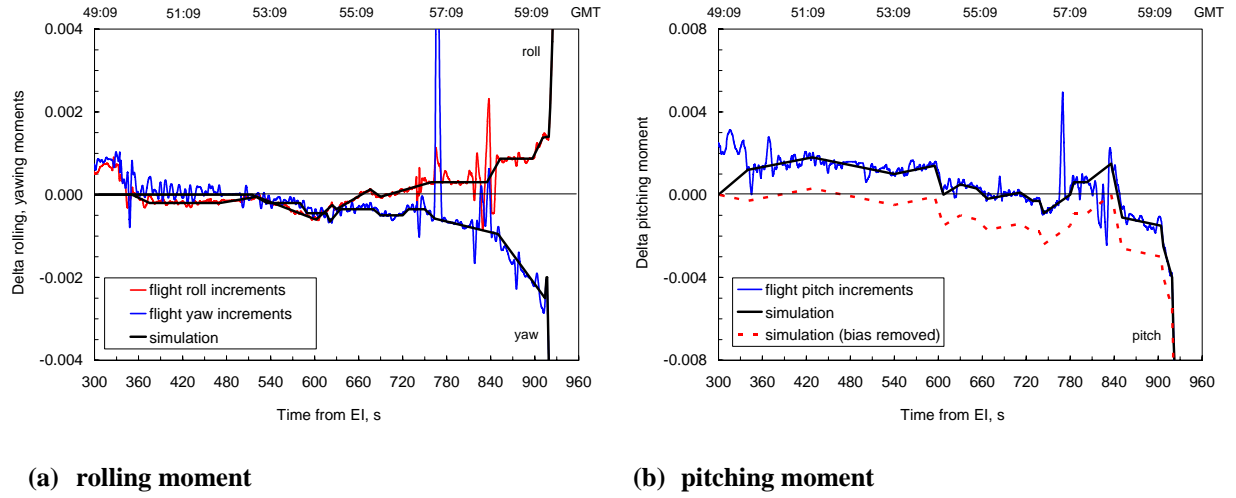
Figure 4.    Extracted incremental flight aerodynamic moments



(a) angle of attack

(b) angle of sideslip

(c) bank angle
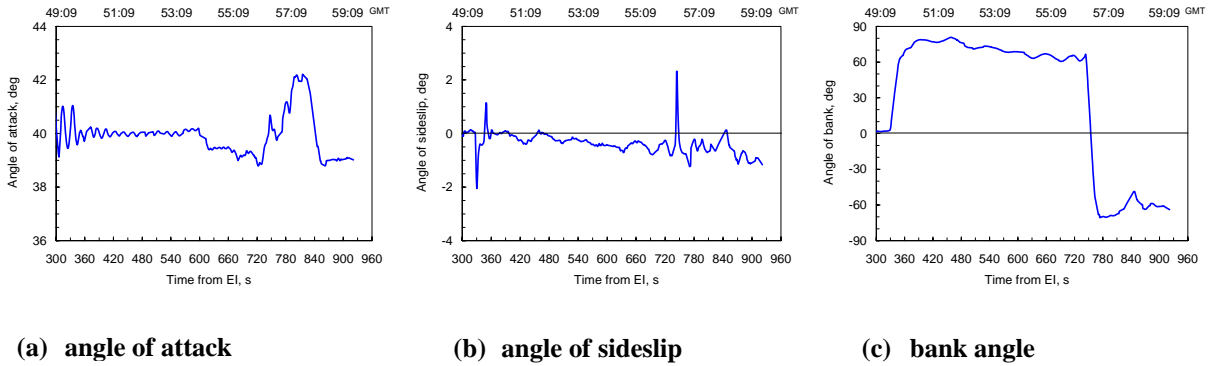
Figure 5.    Extracted flight angles of attack, sideslip and bank

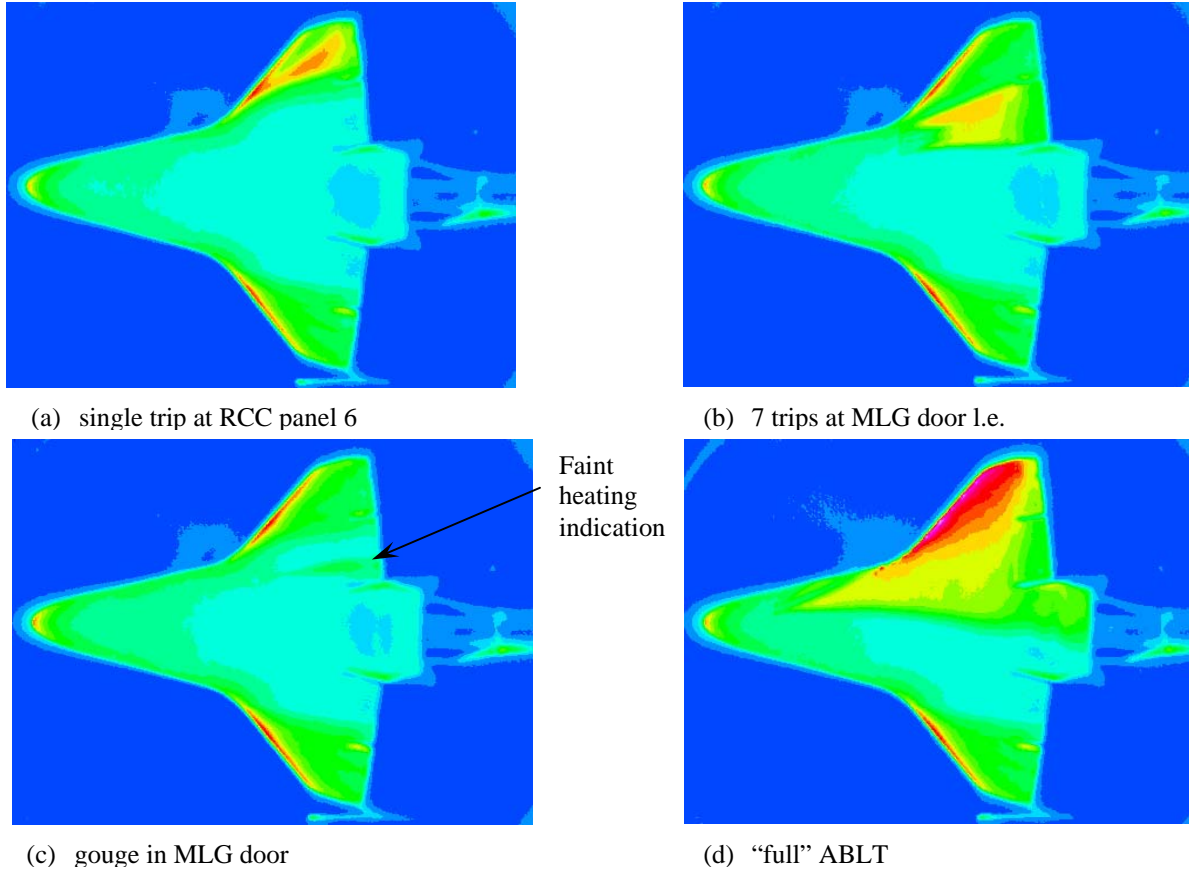## B.  Effect of asymmetric boundary layer transition, trips, and gouges

At the beginning of the investigation the primary area of interest was damage to the acreage tiles on the windward surface of the left wing and the left main landing gear door, and possible early asymmetric boundary layer transition (ABLT) caused by that damage. Boundary-layer transition was initiated in the wind tunnel by using small trips made of Kapton tape with a full-scale height of 0.6 inch. Damage scenarios tested in the Mach 6 air tunnel included a single boundary layer trip at RCC panel 6, a gouge in the center of the main landing gear door (full-scale dimensions approximately 7 by 32 by 4 inches), a raised main landing gear door (raised 1 inch full scale), and 7 trips arrayed span-wise across the leading edge of the door (to further simulate a raised door panel). In addition a "full" asymmetric transition configuration was tested which had 12 trips along the wing leading edge as well as 2 trips well forward near where surface protuberances were observed to cause early transition during flight of STS-28.

The extent of the transitional/turbulent flow generated by these disturbances is shown in Fig. 6a-d for $\alpha = 40°$ and $\beta = 0°$. The "turbulent wedge" from the single trip at RCC panel 6 is swept outboard and affects only the outermost portion of the left wing, as compared to the trips along the forward edge of the main landing gear door, which affect the flow more inboard. These individual trips were more effective than the raised door (image not shown), as the door acted more like a two-dimensional trip or step, which is not as effective in promoting transitional/turbulent flow. The gouge produced non-laminar flow, as a slight increase in heating was observed, but not to the level seen for the raised trips. The "full" asymmetric transition case is seen to provide turbulent flow over

American Institute of Aeronautics and Astronautics

the aft 2/3 of the left side of the model windward surface. The aerodynamic increments generated by these OML changes are shown in Fig. 7a (rolling moment) and Fig. 7b (yawing moment) as a function of angle of attack. The gouge in the door and the raised door had minimal effect on the model aerodynamics. The single trip at RCC panel 6 and the 7 trips at the door leading edge had similar effects to each other, causing a positive rolling moment (right wing down) and a small negative yawing moment (nose left). All increments were less than the "full" ABLT condition. Note the scale used for these and subsequent plots; the magnitudes of the increments are very small.

All the transition-type damage scenarios examined generated incremental rolling and yawing moments consistent in terms of direction with the flight-derived Shuttle ABLT model[13], which is a positive rolling moment (right wing down) combined with a negative (nose left) yawing moment. The ABLT model is conservative in that it bounds the maximum asymmetric moments observed in flight; values for the rolling and yawing moments (roll is same magnitude but opposite sign) vary from 0.0003 at Mach 6 to 0.0015 at Mach 18. The current wind tunnel results at Mach 6 are roughly 0.0005, only slightly greater than the ABLT model, with roll and yaw magnitudes nearly equal. The flight-derived ABLT model and the current wind tunnel results are inconsistent with the extracted STS-107 flight data for the early portion of the flight, which have a left-wing down rolling moment combined with a nose-left yawing moment, indicating that asymmetric transition was not a primary cause of the accident. Furthermore, while boundary layer transition may have been present and could provide for some positive rolling moment when the reversal in rolling moment occurred later, the yawing moment remained relatively flat, suggesting that ABLT was not a major contributor to the rolling moment reversal from an aerodynamic perspective.



   (a)  single trip at RCC panel 6



   (b)  7 trips at MLG door l.e.



   (c)  gouge in MLG door

Faint heating indication



   (d)  "full" ABLT

**Figure 6.   Infra-red images of windward surface with various OML alterations**
**($\alpha = 40°$, $M_\infty = 6$, Air, $Re_{\infty, LB} = 2.4 \times 10^6$)**

(a) rolling moment  (b) yawing moment
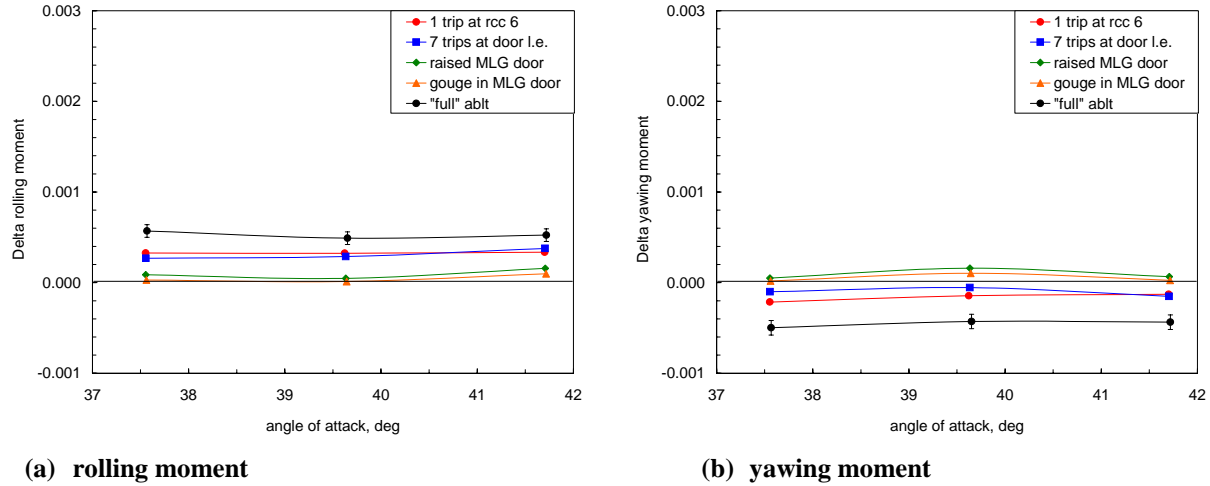
**Figure 7.    Incremental aerodynamic moment coefficients for various OML alterations**
**($M_\infty = 6$, Air, $Re_{\infty, LB} = 2.4 \times 10^6$)**

### C.  Missing full RCC panels

As mentioned in the introduction, two temperature instruments on the left side of the fuselage had experienced significant increases in heating rates roughly 615 seconds after entry interface. Investigators at Langley had modified the wing leading edge with a "notch", both experimentally and computationally, and side fuselage disturbances near these gage locations were produced by both techniques. Given this knowledge, an extensive survey of wing leading edge damage in terms of missing RCC panels was undertaken in the 20-Inch $CF_4$ Tunnel. The $CF_4$ Tunnel, as discussed previously, provides a simulation of Mach 18-24 flight conditions via use of a heavy gas, providing a lower ratio of specific heats which more accurately simulates the flight flowfield in terms of normal shock density ratio, surface pressures, and bow shock/wing shock interaction locations.

The aerodynamic results for single (individual) missing panels as a function of panel location are shown in Fig. 8a-f. Along with the measured data, a linear curve fit to the data is also shown, and for the moments a predicted curve is shown using the fitted force data and appropriate moment arms from the missing panel location to the vehicle moment center. Assuming that side force is negligible (see Fig. 8c), $\Delta Cl \sim \Delta CN * Y_{bar}$, $\Delta Cn \sim \Delta CA * Y_{bar}$, and $\Delta Cm \sim \Delta CA * Z_{bar} + \Delta CN * X_{bar}$, where $X_{bar}$, $Y_{bar}$, and $Z_{bar}$ are the respective moment arms. The normal force increment is small, negative (indicating a loss of lift), and nearly constant with panel location. A loss of lift is expected due to the loss of area, but the situation is more complex as the flow into and out of the notch will affect both the windward and leeside surfaces of the wing, as well as the side of the fuselage. Axial force increases as panel location moves outboard. Rather than the continuous linear trend shown, the axial force appears to reach two distinct levels, one for panels 2-6, and another for panels 8-12. This behavior is attributed to the change in wing sweep from 81° to 45° outboard of panel 7, as a notch in the wing leading edge is then more aligned with the axial direction. The results for rolling moment (Fig. 8d) show a nearly constant negative (left wing down) value for a given missing panel location, while the prediction using the nearly constant normal force increment indicates an increasing left-wing down rolling moment should occur as the moment arm increases. One possible explanation for this difference may be an increased pressure on the outboard wall of the notch providing a positive roll to negate the effect of the normal force. This side force would also counteract any side force due to the increased pressures on the fuselage side from the flow impingement (which causes the heating increase). It should be noted that the actual vehicle would not have solid walls, in that there is an open "chunnel" between the leading edge panels and the front wing spar. However, as this "chunnel" would likely fill with gas rather quickly, a solid wall should be a valid representation. A qualitative heating analysis of the difference between solid and open walls for missing RCC panels showed little effect on the leeside heating patterns[6]. Delta yawing moment (Fig. 8e) exhibited a relatively strong dependence on missing panel location, with a more nose-left yawing moment generated for the more outboard locations. In this case the force data adequately predicts the moment data. Delta pitching moment (Fig. 8f) shows a dependence on missing panel location also, as nose-down pitch increased for more outboard panel locations. The

American Institute of Aeronautics and Astronautics

curve upward of the prediction for RCC panels greater than 6, and possibly observed for panel 12, is due to the location of the RCC panels being forward, then aft of the vehicle moment center (see Fig. 1).

Data for a series of tests with multiple missing RCC panels are presented in Fig. 9a-c; data for missing panels 6, 6-7, 5-7, 5-8, and 5-9 are shown. Superposition of the increments for single missing RCC panels (using the linear fit) was fairly successful in predicting multiple-panel out increments; the trends were captured and often so were the magnitudes. The flight delta aerodynamic data are also shown for comparison as a function of time from entry interface. The small magnitude of the early flight values indicate that the damaged area in flight was not far outboard, or was smaller than an entire missing RCC panel; and the delta roll, delta yaw, and delta pitch increments all become progressively more negative (left wing down, nose left, nose down) as the number of missing panels is increased. In flight, however, the roll trend reversed, indicating that something occurred other than, or in addition to, a continuing loss of leading edge panels.
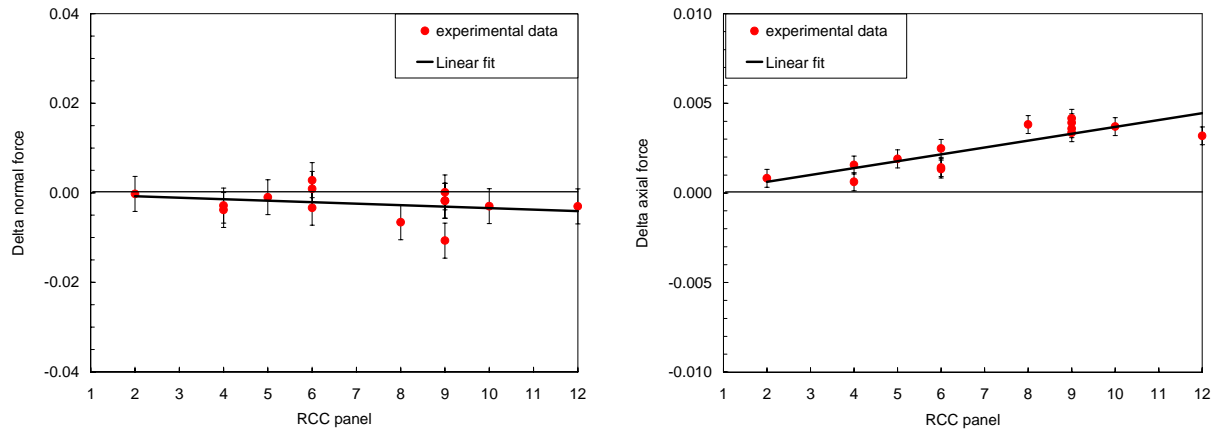


(a) normal force



(b) axial force

**Figure 8.    Incremental aerodynamic coefficients for individual completely missing RCC panels**
**($\alpha = 40°$, $CF_4$, $Re_{\infty, LB} = 0.4 \times 10^6$)**
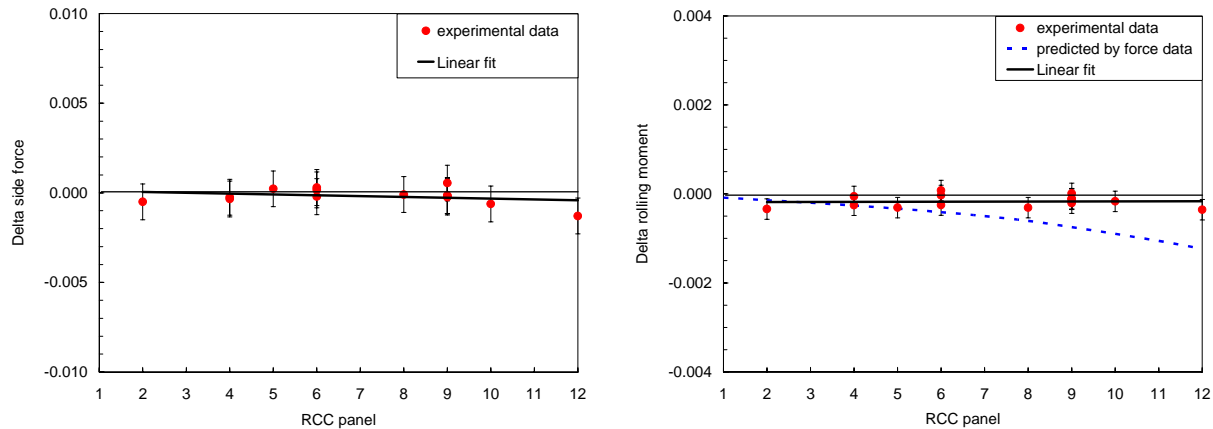


(c) side force



(d) rolling moment

**Figure 8.    Continued.**
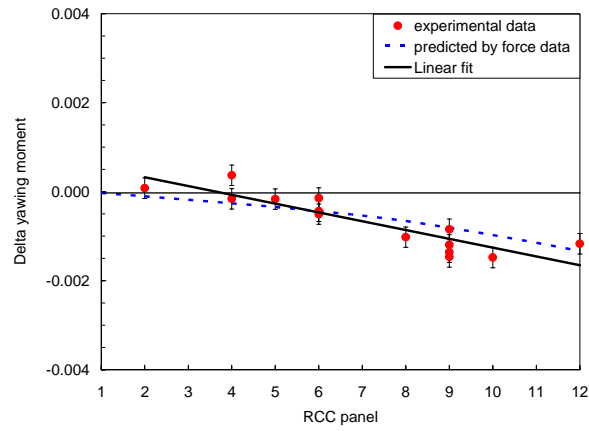
**(e) yawing moment**
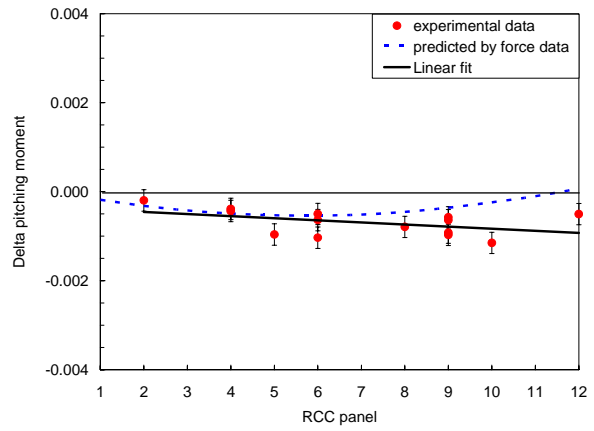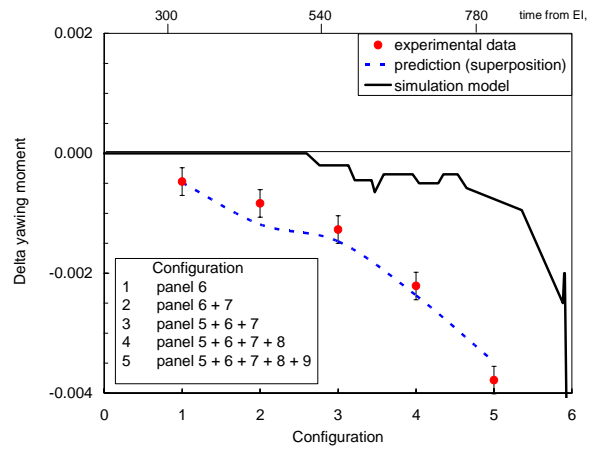
**(f) pitching moment**
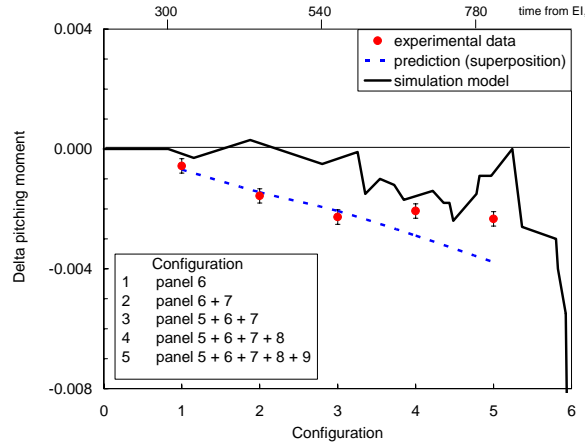
**Figure 8.   Concluded.**
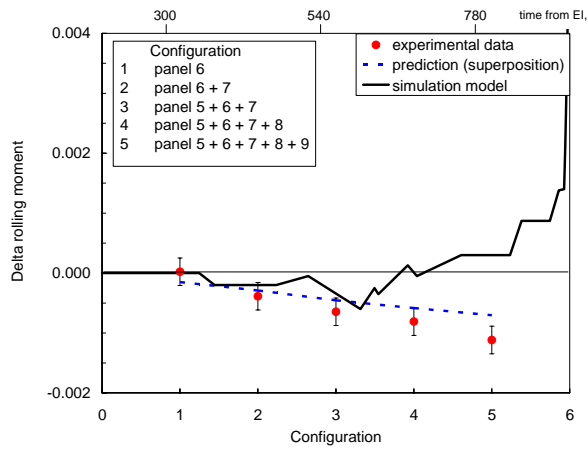


**(a) rolling moment**

**(b) yawing moment**

**Figure 9.   Incremental moment coefficients for multiple completely missing RCC panels**
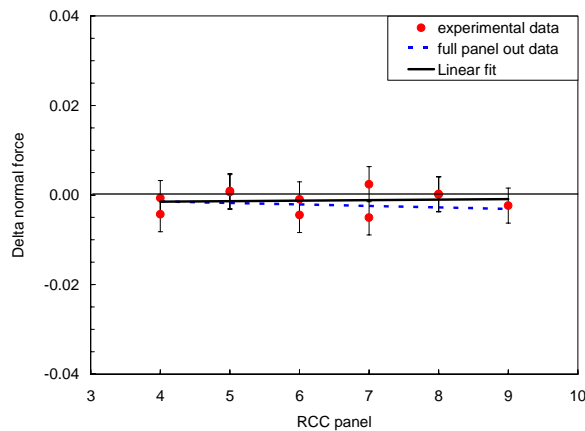**($\alpha = 40°$, $CF_4$, $Re_{\infty, LB} = 0.4 \times 10^6$)**
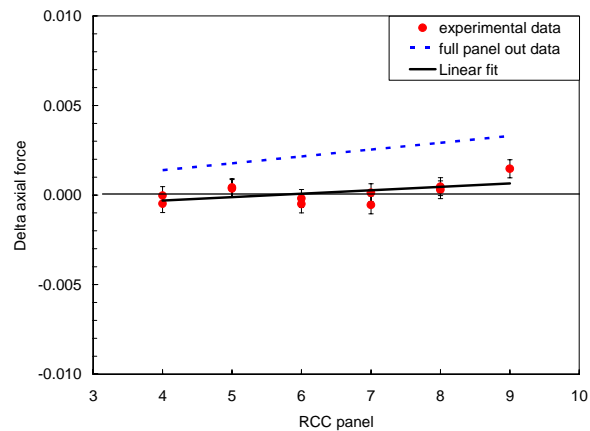
**(c) pitching moment**

**Figure 9.   Concluded.**

## D.  Missing partial RCC panels

As more of the debris was recovered and analyzed, a scenario emerged that a partially damaged RCC panel or panels may more appropriately model the actual damage, as opposed to a full panel missing. A series of tests was undertaken to examine the effect of a missing lower portion of a RCC panel. The wing leading edge was modified by removing the lower portion of the panel from the wing apex to the start of the lower carrier panel. The aerodynamic results for individually removed lower panels 4 through 9 are shown in Fig. 10a-f. For comparison, the linear fit to the full panel out data presented in the previous section is shown by the dashed line. Overall, the magnitudes of the incremental forces and hence moments for missing partial panels were smaller than those for a full missing panel. The axial force increment is substantially less. This may be expected as the damaged area exposed to the flow in the axial direction is less than for a full missing panel. There is negligible effect of a partial missing panel on normal force, side force, and rolling moment. Axial force, yawing moment, and pitching moment show a slight effect, mainly for the more outboard panel locations.
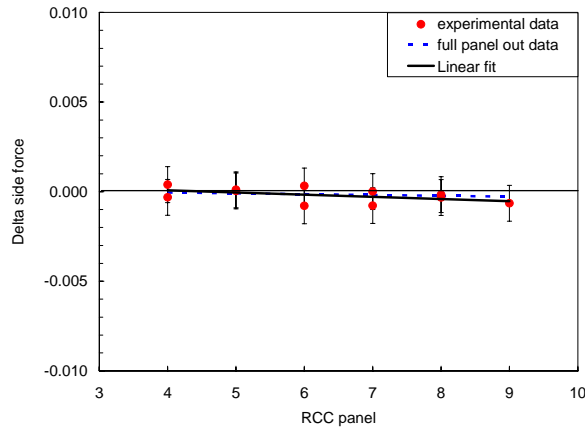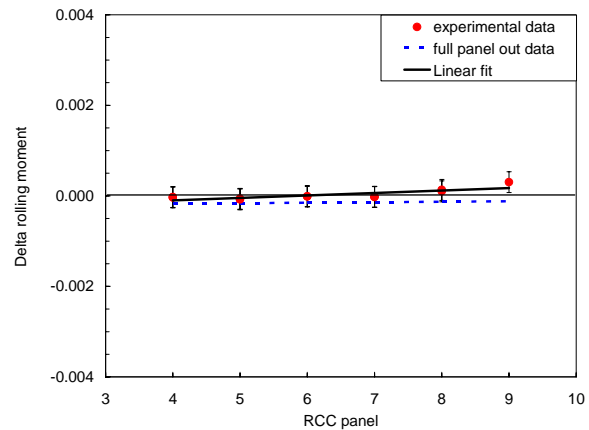


**(a)  normal force**



**(b)  axial force**

**Figure 10.   Incremental aerodynamic coefficients for individual partially missing RCC panels**
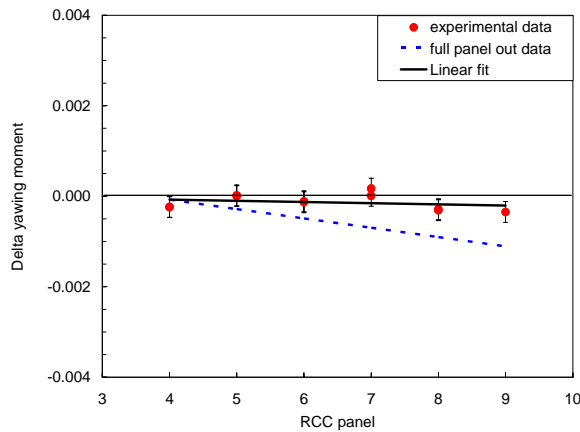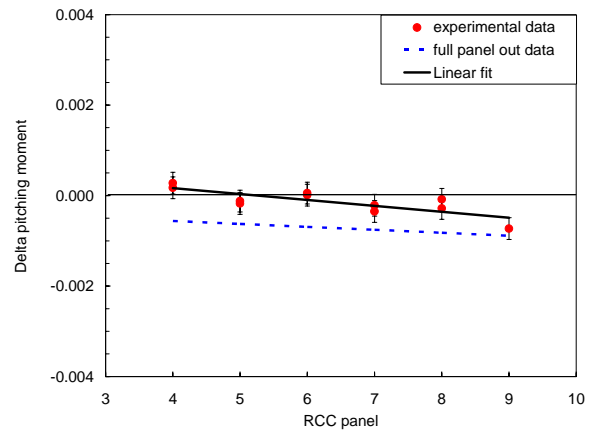**($\alpha = 40°$, $CF_4$, $Re_{\infty, LB} = 0.4 \times 10^6$)**

13
American Institute of Aeronautics and Astronautics

**(c) side force**



**(d) rolling moment**

**Figure 10. Continued.**
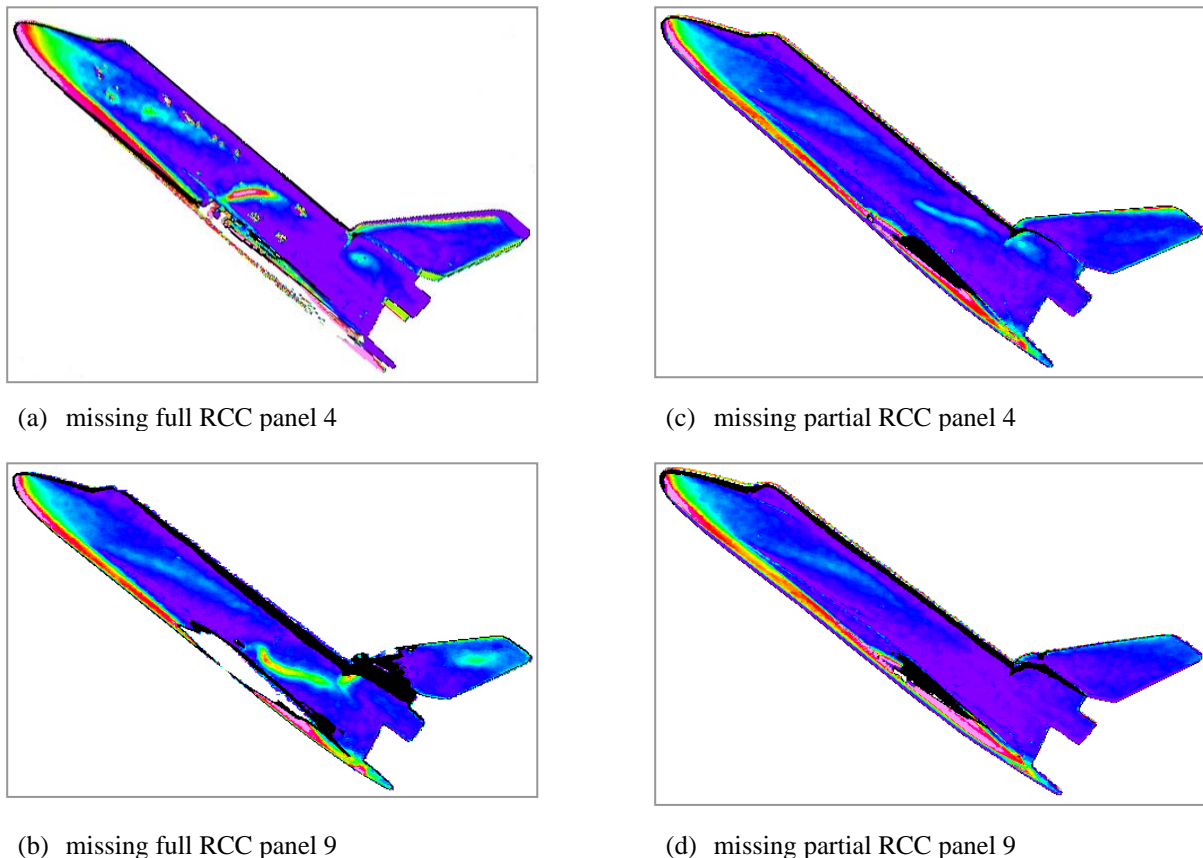


**(e) yawing moment**



**(f) pitching moment**

**Figure 10. Concluded.**

**E. Flow to the leeside via holes and slots through the wing**

A recurring question during the investigation was what wing leading edge or windward surface damage scenario would provide aerodynamic characteristics observed in flight and simultaneously generate the leeside disturbances (side fuselage heating) observed in flight. This leeside disturbance had been shown to be possible for a full missing panel. However, for partially missing panels, flow did not impinge on the leeside fuselage for the more outboard panels. The determining factor was the panel location relative to the attachment line on the windward surface[6]. The attachment line is simply the dividing line where flow either wraps around the leading edge to the leeside or remains on the windward surface. Phosphor thermography images were taken for the series of missing lower RCC panels. Figure 11a-d shows the results for panels 4 and 9 for both full and partially missing panels. For full missing panels 4 and 9, as well as partial missing panel 4, a disturbance is seen on the leeside fuselage; but no such disturbance is observed for partial missing panel 9. An alternate path for flow to reach the leeside that was examined was holes or

slots through the wing from windward to leeward (upper) surface. For one series of tests, small holes (0.030-in diameter model scale, 4 in diameter full scale) were drilled through the wing from the windward surface to the leeside at the carrier panel locations behind RCC panels 6, 9, and 12 (separate runs), but did not include missing panels nor other alterations. No effect of these holes through the wing was observed in either the aerodynamic increments or the side fuselage images. For another series of tests, a 0.030-inch hole was drilled from the windward surface, at the center, aft end of partial missing panel 8, to the leeside through upper carrier panel 8. Afterwards this hole was widened to a 0.030-inch slot, in effect removing most of the upper carrier panel. Phosphor thermography images of the fuselage side are shown in Fig. 12a-c. A slight effect on heating to the OMS pod can be seen for the single hole. The slot resulted in increased heating on the side of the fuselage and the OMS pod, similar to that observed for a full missing panel, though the heating rate is lower (approximately 30% of the heating rate with a full missing panel 9). The aerodynamic increments in rolling and pitching moments associated with the hole and slot are very small, but there is a measurable increase in the nose-left yawing moment increment when the hole is widened to a slot (Fig. 13).



(a)  missing full RCC panel 4



(c)  missing partial RCC panel 4



(b)  missing full RCC panel 9



(d)  missing partial RCC panel 9

**Figure 11.  Thermographic phosphor images for full and partially missing RCC panels**
**($\alpha = 40°$, $CF_4$, $Re_{\infty, LB} = 0.4 \times 10^6$)**
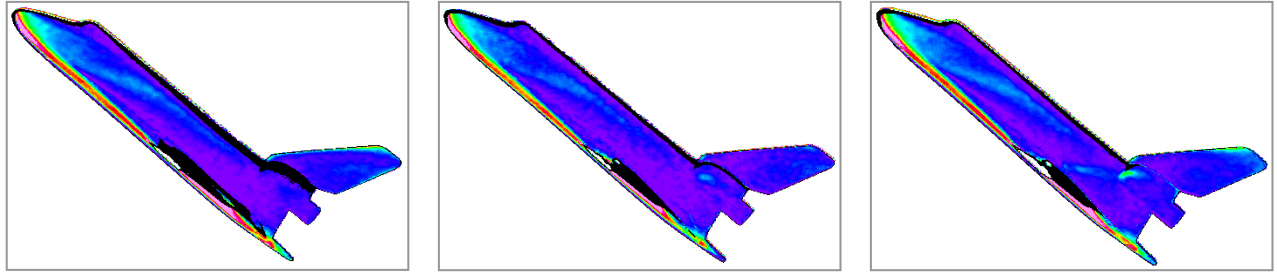
(a) missing lower RCC panel 8     (b) missing lower RCC 8 with hole     (c) missing lower RCC 8 with slot

**Figure 12.  Thermographic phosphor images for holes and slots through left wing**
**($\alpha$ = 40°,  CF$_4$, Re$_{\infty, \text{LB}}$ = 0.4 x10$^6$)**
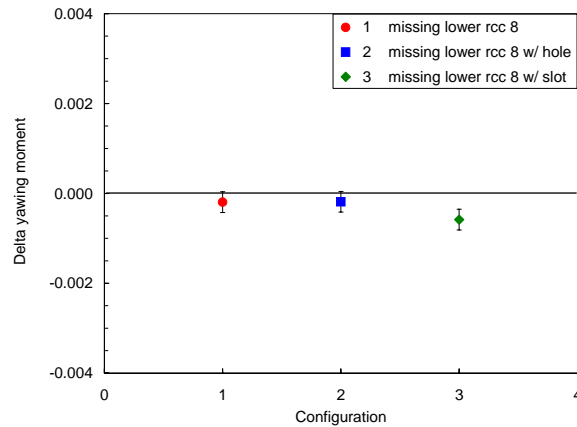


**Figure 13.  Yawing-moment increment for holes and slots through left wing**
**($\alpha$ = 40°,  CF$_4$, Re$_{\infty, \text{LB}}$ = 0.4 x10$^6$)**

**F.  Effect of flow impingement on the vertical tail**

The effect of possible flow impingement on the vertical tail was investigated for several reasons: phosphor thermography images show increased heating on the tail for several damage scenarios, physical damage was noted on the recovered debris with substantially more damage on the left side than on the right, and the tail was seen as a possible contributor to the large roll and yaw increments seen late in flight, and especially for the change in rolling moment behavior. The tail has a large area and moment arms, thus a small change in pressure could have a measurable effect on the aerodynamic forces and moments. A model was tested with the tail on and off, with and without RCC panel 9 missing. As shown in Table 3, the increments (between results with and without RCC panel 9) with and without the vertical tail are very close in value, leading to the conclusion that the tail was not a contributor to the moments in question.

Table 3: Effect of vertical tail with and without missing RCC panel 9; 20-Inch $CF_4$ Tunnel

| Run | Tail | $\alpha$ (deg) | $Re_\infty$ $(ft^{-1})$ | $\Delta Cl$ | $\Delta Cn$ | $\Delta Cm$ | $\Delta CY$ |
|---|---|---|---|---|---|---|---|
| 1 | on | 40.2 | 0.45 | -0.00006 | -0.00115 | -0.00105 | 0.00013 |
| 2 | on | 40.5 | 0.46 | 0.00007 | -0.00131 | -0.00128 | -0.00037 |
| 3 | on | 40.5 | 0.45 | 0.00008 | -0.00132 | -0.00128 | 0.00022 |
| 1 | off | 40.5 | 0.46 | -0.00007 | -0.00122 | -0.00125 | -0.00006 |
| 2 | off | 40.5 | 0.44 | -0.00013 | -0.00122 | -0.00117 | 0.00006 |
| average | on | 40.4 | 0.45 | 0.00003 | -0.00126 | -0.00120 | -0.00001 |
| average | off | 40.5 | 0.45 | -0.00010 | -0.00122 | -0.00121 | 0.00000 |
| delta | | -0.1 | 0.00 | 0.00013 | -0.00004 | 0.00001 | -0.00001 |

## G. Reynolds number effects

A brief series of tests examined Reynolds number effects. Missing RCC panel 9, and missing RCC panels 6 and 9 together, were tested at two Reynolds numbers, 0.27 and 0.46 per foot. The results, summarized in Table 4, reveal no significant Reynolds number effect for this factor-of-two variation in Reynolds number.

Table 4: Effect of Reynolds number; 20-Inch $CF_4$ Tunnel

| Run | Configuration | $\alpha$ (deg) | $Re_\infty$ $(ft^{-1})$ | $\Delta Cl$ | $\Delta Cn$ | $\Delta Cm$ |
|---|---|---|---|---|---|---|
| A | missing RCC 9 | 39.5 | 0.27 | -0.00018 | -0.00119 | -0.00081 |
| B | missing RCC 9 | 40.1 | 0.45 | -0.00012 | -0.00119 | -0.00092 |
| | delta | | | 0.00006 | -0.00001 | -0.00011 |
| C | missing RCC 6 and 9 | 39.5 | 0.28 | -0.00045 | -0.00133 | -0.00151 |
| D | missing RCC 6 and 9 | 40.1 | 0.45 | -0.00034 | -0.00139 | -0.00168 |
| | delta | | | 0.00010 | -0.00006 | -0.00017 |

## H. Main landing gear deployment

The effect of deploying the main landing gear and door was tested in the $CF_4$ tunnel, as well as the Mach 6 air tunnel. Although not a primary candidate as an initiating event, this scenario was examined as a possible explanation for the large aerodynamic moments observed near the time of loss of signal. Configurations consisting of an open wheel well (no door) of several depths, a door alone, gear alone, and door and gear deployed were tested. Filler plates were used to create three different depths of the open wheel well in order to simulate the presence of the gear (the presence of the gear would tend to fill the wheel well, in essence making the cavity shallower). A sketch of these configurations was shown in Fig. 1. Similar results in terms of delta rolling, yawing, and pitching moments were observed in both air and $CF_4$ for these configurations as shown in Fig. 14a-c, with the exception that the roll and pitching moments were much greater in air when the gear was deployed. The difference, as shown in the Schlieren photographs shown in Fig. 15, is attributed to the gear extending through the shock layer into the freestream flow in $CF_4$, while in air the bow shock appears to impinge on the wheel (the bow shock lies closer to the body in the $CF_4$ tunnel and in flight, compared to air); the door is within the shock layer for both test gases. Also shown is the prediction of the $CF_4$ experimental data using the incremental force data and appropriate moment arms (center of wheel well or door, and gear location). The prediction is reasonable for roll and yaw; however pitching moment is not predicted well except for the open cavity configurations. Note also that the pitching moment is nose-

up for the gear/door configurations, which is unexpected in that the increased axial load acting on the gear would tend to pitch the Orbiter nose-down. A possible explanation is that the door and gear cause local increases in pressure ahead of the moment center, as well as decreases in pressure in the downstream wake over the aft area of the wing. This moment-couple effect would lessen the normal increment while still causing the pitch-up moments observed. The $CF_4$ data is shown again in Fig. 16a-c compared to the flight data. The open wheel well configurations (lines A and B) have increasing magnitudes for all three moments as the cavity is made shallower, and the trend is in the same direction as flight. This behavior is consistent with "open" and "closed" type cavity flows, where for deeper cavities some flow re-circulates within the cavity, but the main flow essentially passes over the cavity; as the depth is decreased, the flow impinges on and attaches to the cavity floor, a shock (observed in the Mach 6 air tunnel) is formed as the flow reaches the aft wall, and the pressure on the cavity floor and aft wall is significantly increased. This increased pressure may generate the moments observed. The door and/or gear combinations (lines D and E) generate large rolling and yawing moments consistent with magnitudes later in flight, but the pitching moments are in the opposite direction than those inferred from flight measurements.



(a)  rolling moment

(b)  yawing moment
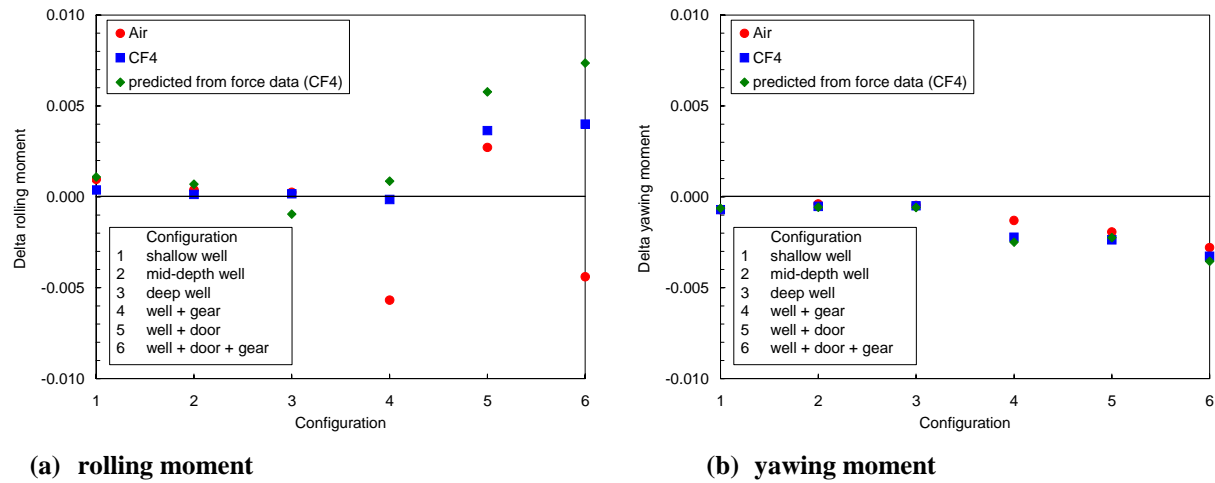
Figure 14.   Comparison of incremental moments in air ($\alpha = 40°$, $M_\infty = 6$, $Re_{\infty, LB} = 2.4 \times 10^6$) and $CF_4$ ($\alpha = 40°$, $Re_{\infty, LB} = 0.4 \times 10^6$) for various landing gear configurations

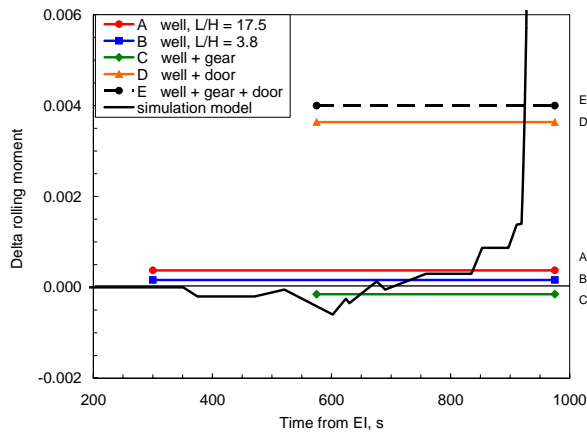

(c)  pitching moment
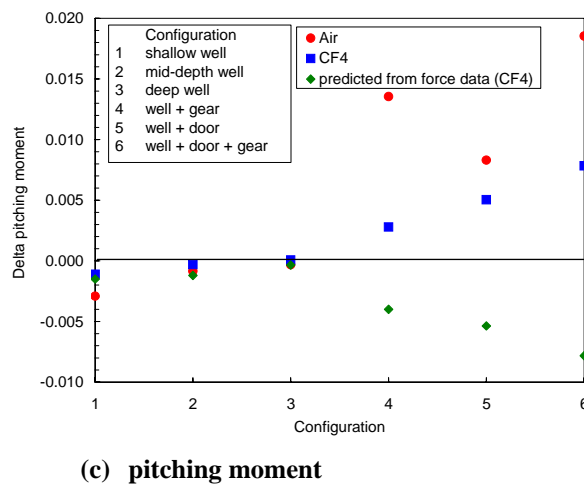
Figure 14.   Concluded.
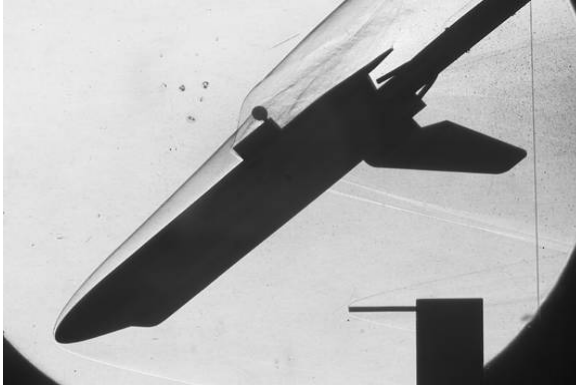
**(a) Mach 6 Air Tunnel**
$\rho_2/\rho_\infty = 5.3$, $\gamma_\infty = 1.40$, $Re_{\infty, LB} = 2.4 \times 10^6$
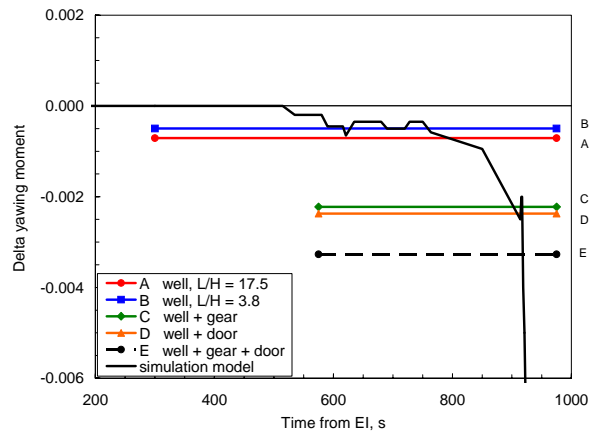
**(b) CF$_4$ Tunnel**
$\rho_2/\rho_\infty = 11.7$, $\gamma_\infty = 1.21$, $Re_{\infty, LB} = 0.4 \times 10^6$

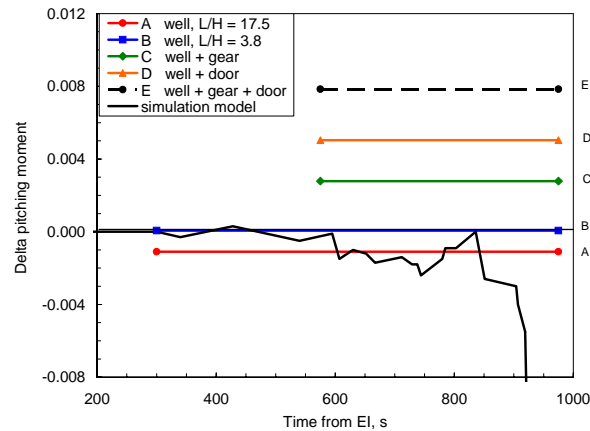**Figure 15. Comparison of Schlieren images in air and CF$_4$ for gear and door deployed ($\alpha = 40°$)**



**(a) rolling moment**

**(b) yawing moment**

**Figure 16. Incremental moment coefficients for various landing gear configurations**
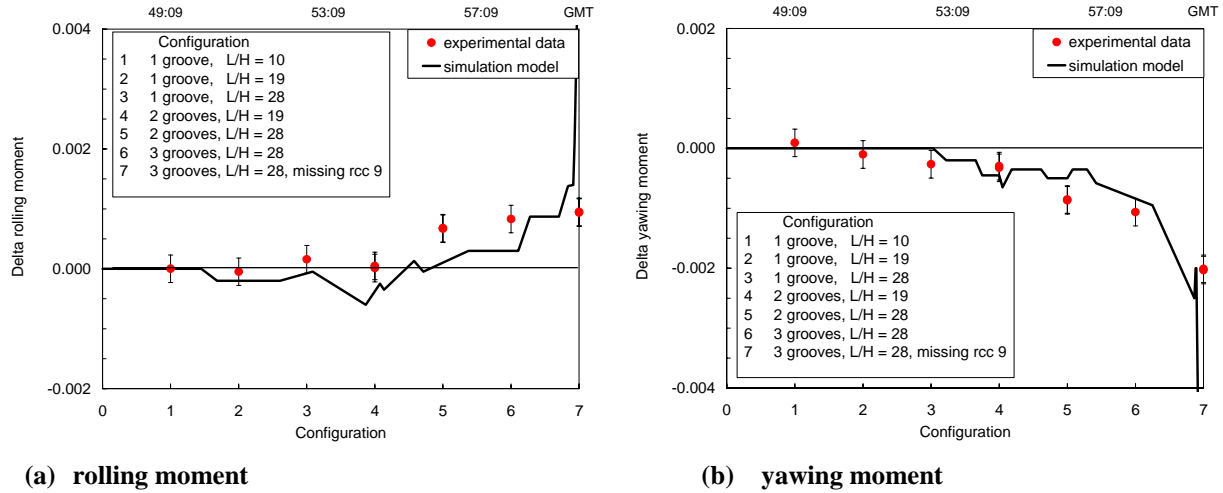**($\alpha = 40°$, CF$_4$, $Re_{\infty, LB} = 0.4 \times 10^6$)**

**(c)    pitching moment**

**Figure 16.   Concluded.**

## I.   Windward surface depression

A final series of aerodynamic tests were performed to determine if a damage scenario related to deformation of the left wing would cause the change in direction of the rolling moment seen to occur 615 seconds after entry interface. A shallow depression was created in the left wing windward surface to simulate what might occur as the wing internal structure was degraded and the windward surface was pressed inward as the external surface pressure exceeded the internal pressure.  A single groove was milled into the lower surface of the model, starting just behind RCC panel 8. The length of this groove was varied in three increments with the longest groove extending slightly past the aft end of the wheel well. This groove was then widened to simulate progressive damage, first inboard to the wheel well location, then outboard. Measured aerodynamic moments show (Fig. 17a-c) that a minimum length of the groove is needed to provide a measurable increase in rolling moment, similar to the critical depth of the open wheel well. The required aspect ratio (L/H) of the groove is greater than for the open wheel well; this effect may be related to the angle of the local streamlines, in that they will cross the groove as opposed to running parallel to it, thus in effect shortening the groove and reducing the aspect ratio. In any case, the depression does indeed cause a positive (right wing down) rolling moment as observed in flight, and the magnitude of the rolling moment increases as the width of the depression is increased. Furthermore, the yawing moments and pitching moments generated by the depression are similar in magnitude and in the same direction as observed for flight.

**(a)  rolling moment**

**(b)  yawing moment**

**Figure 17.  Incremental moment coefficients for various windward surface damage scenarios**
$(\alpha = 40°, CF_4, Re_{\infty, LB} = 0.4 \ x10^6)$
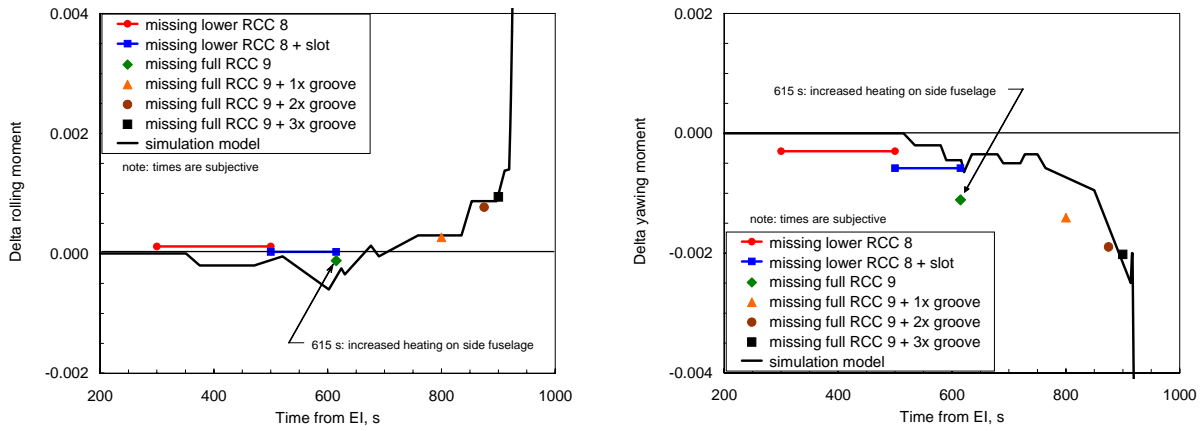


**(c)  pitching moment**
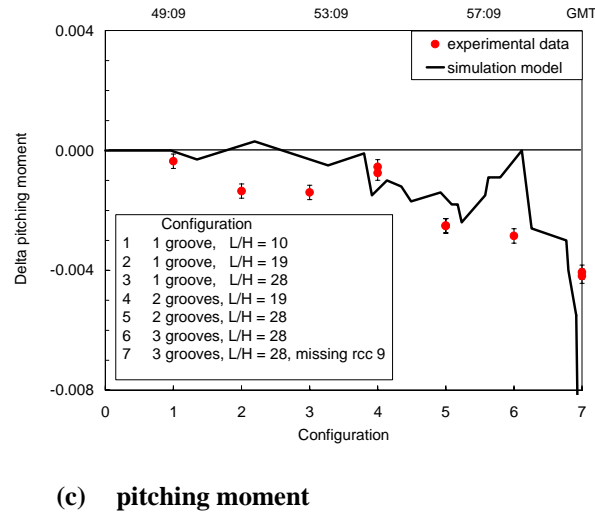
**Figure 17.  Concluded.**

## J.  Progressive damage scenario

As a final summation to the aerodynamic work, a progressive build-up of individual damage scenarios was developed and compared to the flight moment increments. The results are shown in Fig. 18a-c. The selected times from entry interface are subjective, as are the damage scenarios themselves. Nonetheless, a plausible scenario is developed, which has the same trends as the flight data, although an exact correlation of flight magnitudes and time is not achieved. The initial damage is loss of the lower portion of RCC panel 8. The magnitudes of the moment increments are small, as they were for the first 500 seconds or so of flight. This initial damage is followed by the addition of the slot through the upper portion of carrier panel 8, and then the complete removal of panel 9 at 615 seconds from entry interface (EI). It was at this time (615 seconds) that significant heating to the side fuselage was seen, and both the slot in carrier panel 8 and the complete removal of panel 9 allow flow to impinge on the leeside of the vehicle. The reversal in direction of the rolling moment is attributed to the windward surface depression, with
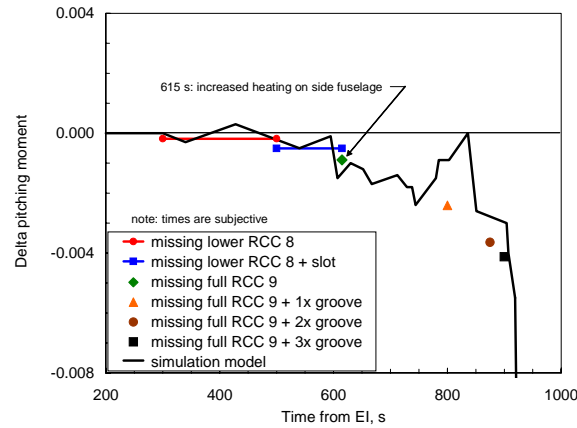
the magnitude increasing as the size of the depression is increased (as more of the internal wing structure is degraded). The yawing and pitching moments continue their increasing negative trend as the depression is enlarged.



(a) rolling moment



(b) yawing moment

**Figure 18.   Incremental moment coefficients for progressive damage scenario**
        $(\alpha = 40°, CF_4, Re_{\infty, LB} = 0.4 \times 10^6)$



(c) pitching moment

**Figure 18.   Concluded.**

## V.    Conclusions

Aerodynamic tests in support of the *Columbia* accident investigation were conducted in two hypersonic wind tunnels at the NASA Langley Research Center, the 20-Inch Mach 6 Air Tunnel and the 20-Inch $CF_4$ Tunnel. The forces and moments generated by a variety of outer mold line alterations (damage scenarios) were measured using 0.0075-scale models of the Space Shuttle Orbiter. Complementary global heat transfer mappings were simultaneously acquired for a majority of the configurations tested. The damage scenarios evaluated included asymmetric boundary layer transition, gouges in the windward surface acreage thermal protection system tiles, wing leading edge damage (partially and fully missing reinforced carbon-carbon (RCC) panels), holes through the wing from the windward surface to the leeside, deformation of the wing windward surface, and main landing gear door

and/or gear deployment. The aerodynamic data were compared to the magnitudes and directions observed in flight, and the heating images were evaluated in terms of the location of the generated disturbances and how these disturbance might relate to the response of discrete gages on the Columbia Orbiter vehicle during entry.

The measured aerodynamic increments in general were small in magnitude, as were the flight-derived values during most of the entry. Asymmetric boundary layer transition (ABLT) results were consistent in sign with the flight-derived Shuttle ABLT model, but not with the observed flight trends for STS-107, suggesting that ABLT did not play a significant role in the loss of *Columbia*. Full missing RCC panels had yawing moments that increased when damage moved more outboard on the wing, as expected, but rolling moments did not. Partial missing RCC panels had smaller aerodynamic increments than the full missing panels, as expected. Deployment of the landing gear resulted in aerodynamic moments of relatively larger magnitudes as observed late in flight near the time of loss of signal, but the direction was opposite, indicating the gear did not deploy during entry. The partially missing leading edge panel scenario best matched both the aerodynamic and heating trends observed early in flight (small aerodynamic moments with flow impingement increasing the heating on the leeside fuselage), and the recovered debris on the ground (a portion of most RCC panels was recovered). Damage to the windward surface in the form of grooves caused aerodynamic moments similar to those which occurred during later times in flight, and notably a positive rolling moment which had not been produced by damage scenarios investigated to that time. A progressive damage scenario was presented that qualitatively matches the aerodynamic flight observations (rolling, yawing, and pitching moments) for the entire trajectory: loss of the lower portion of RCC 8, loss of the upper carrier panel behind RCC 8 (slot through the wing), loss of full RCC panel 9, a windward surface depression, and growth of the windward surface depression.

## VI.    References

[1]Columbia Accident Investigation Board Report, Volume I, August 2003.

[2]Miller, C. G., "Langley Hypersonic Aerodynamic/Aerothermodynmaic Testing Capabilities – Present and Future," AIAA 90-1376.

[3]Brauckmann, G.J., Paulson, J. W. Jr., and Weilmuenster, K. J., "Experimental and Computational Analysis of Shuttle Orbiter Hypersonic Trim Anomaly," *Journal of Spacecraft and Rockets*, Vol. 32, No. 5, September-October 1995.

[4]Berry, S. A., and Hamilton, H.H., "Discreet Roughness Effects on Shuttle Orbiter at Mach 6", AIAA 2002-2744, June 24-27, 2002.

[5]Berry, S. A., Bouslog, S. A., Brauckmann, G. J., and Caram, J. M., "Shuttle Orbiter Experimental Boundary-Layer Transition Results with Isolated Roughness," *Journal of Spacecraft and Rockets*, Vol. 35, No. 3, 1998, pp. 241-248.

[6]Horvath, T.J., "Experimental Aerothermodynamics in Support of the Columbia Accident Investigation," AIAA 2004-1387, January 5-8, 2004.

[7]Buck, G. M., "Rapid Model Fabrication and Testing for Aerospace Vehicles," AIAA 2000-0826.

[8]Buck, G. M., and Vasquez, P., "An Investment Ceramic Slip Casting Technique for Net-Form, Precison, Detailed Casting of Ceramic Models," U.S. Patent 5,266,252.

[9]Daryabeigi, K., Berry, S. A., Horvath, T. J., and Nowak, R. J., "Finite Volume Numerical Methods for Aeroheating Rate Calculations from Infrared Thermographic Data," AIAA 2003-3634.

[10]Merski, N. R., "Reduction and Analyisis of Phosphor Thermographgy Data with the IHEAT Software Package," AIAA 98-0712.

[11]Merski, N. R., "Global Aeroheating Wind-Tunnel Measurements Using Improved Two-Color Phopshor Thermography Method," *Journal of Spacecraft and Rockets*, Vol. 36, No. 2, 1998.

[12]NSTS-37398, "Aero/Aerothermal/Thermal/Structures Team Final Report in Support of the Columbia Accident Investigation," August 6, 2003.

[13]An, M. Y., Wang, K. C., Campbell, C. H., and Pelley, R. L., "Space Shuttle Orbiter Aerodynamics Induced by Asymmetric Boundary-Layer Transition," AIAA 96-0808, January 15-18, 1996.